Available online at www.sciencedirect.com
ScienceDirect
Trans. Nonferrous Met. Soc. China 31(2021) 1612−1627
Transactions of Nonferrous Metals Society of China
www.tnmsc.cn

In-situ layered double hydroxides on Mg−Ca alloy: Role of calcium in magnesium alloy

Yu XIA[1], Liang WU[1,2], Wen-hui YAO[1,2], Meng HAO[1], Jing CHEN[1], Cheng ZHANG[3], Tao WU[1], Zhi-hui XIE[4], Jiang-feng SONG[1,2], Bin JIANG[1,2], Yan-long MA[5], Fu-sheng PAN[1,2]

1. State Key Laboratory of Mechanical Transmission, College of Materials Science and Engineering, Chongqing University, Chongqing 400044, China;
2. National Engineering Research Center for Magnesium Alloys, Chongqing University, Chongqing 400044, China;
3. The Key Laboratory of Chongqing Inorganic Special Functional Materials, School of Materials Science and Engineering, Yangtze Normal University, Chongqing 408100, China;
4. Chemical Synthesis and Pollution Control Key Laboratory of Sichuan Province, College of Chemistry and Chemical Engineering, China West Normal University, Nanchong 637002, China;
5. College of Materials Science and Engineering, Chongqing University of Technology, Chongqing 400054, China

Received 23 May 2020; accepted 28 January 2021

Abstract: Mg−Al layered double hydroxides (LDHs), produced on cast Mg−*x*Ca (*x*=0.5, 0.8, 2.0, wt.%) alloys by an in-situ growth method, showed good corrosion resistance compared to the bare magnesium substrate. The influence mechanism of the second phase (Mg_2Ca) on LDHs production was investigated. Increasing Ca content increased the amount of Mg_2Ca, decreasing the grain size and the corrosion rate of the alloys. The increased amount of the second phase particles and the grain refinement promoted the growth of LDHs, and thus led to the decreasing of corrosion rate of the Mg−*x*Ca alloys with LDHs. A higher Mg_2Ca amount resulted in forming fluffy LDHs. Due to the dual effects of the second phase (Mg_2Ca) for LDHs growth and microgalvanic corrosion, LDHs/Mg−0.8Ca showed the lowest corrosion rate.

Key words: Mg−Ca alloys; Mg−Al layered double hydroxides; corrosion resistance; in-situ growth; self-healing

1 Introduction

Magnesium alloys have significant applications in the automotive and aerospace industries, and for electronic products, aerospace, implant applications and other fields because of their advantages of low density, high specific strength, high thermal conductivity, bio-compatibility, biodegradability, and environmental friendliness [1−5]. However, their poor corrosion performance limits their more widespread applications [6−10].

Currently, there are two primary research directions to improve the corrosion performance of Mg alloys. One method is by alloying [5] with elements, such as Ca, Mn and Zn elements [11−13]. Alloying with Ca is of particular interest for the corrosion of magnesium alloys [14]. Ca with a low density (1.55 g/cm^3), is a crucial factor for human bone, and hydroxyapatite (HA) produced during corrosion of Mg−Ca alloys in the body accelerates bone healing [13,15], which enables applications of Mg−*x*Ca alloys in bio-materials [16]. Nevertheless, there has been exceedingly few Mg alloys that have a corrosion rate lower than the intrinsic corrosion rate by mass loss of 0.3 mm/a in a technically relevant solution such as a concentrated chloride

Corresponding author: Liang WU, E-mail: wuliang@cqu.edu.cn
DOI: 10.1016/S1003-6326(21)65602-9

solution. The second research direction is surface treatment. There are many kinds of common anti-corrosion coatings, including chemical conversion coatings [17], micro-arc oxidation (MAO) [18,19], anodic oxidation [20−22], polymer films [23,24], silane films [25] and electroless coatings [26]. However, in practice, if the coating is damaged, the substrate corrosion is locally accelerated due to the effect of the large cathode and small anode, potentially causing the corrosion protection failure. Consequently, coatings with active corrosion inhibition have attracted great attention [27].

Layered double hydroxides (LDHs), widely researched for corrosion protection coatings, can carry active corrosion inhibitors because of their ability of ion exchange [28,29]. Recently, some LDHs produced on magnesium alloys demonstrated unique corrosion resistance [30−34]. LI et al [30] and KUZNETSOV et al [31] prepared ZnAl−LDHs with vanadate anions via ion-exchange on an anodic layer and achieved active corrosion protection. SERDECHNOVA et al [32] and DOU et al [33] found good corrosion resistance for LDHs on a ceramic-like coating. Moreover, MOHEDANO et al [34] found that PEO/LDHs composite coatings provided good corrosion protection. Furthermore, CHEN et al [35] found that corrosion performance was improved by the faster growth by optimized casting processes. ZHANG et al [36] found that the LDH film growth could be influenced by dislocations, twins, grain boundaries and grains with high electrochemical activity, and the micro-cathode effect of the β-$Mg_{17}Al_{12}$ phase on the alloy surface caused the formation of the LDHs coating preferentially on the α-Mg phase and then on the β-$Mg_{17}Al_{12}$ phase.

The corrosion resistance of magnesium alloys was studied and improved by different methods and processes. However, it is not well understood why the second phase is generally important for the good performance of LDHs. Therefore, further study needs to be conducted to understand how the second phase and grain size of magnesium alloys affect the growth and corrosion resistance of LDHs.

In this work, Mg−Al LDHs were produced on Mg−xCa alloys by the in-situ growth method. The effects of the Ca content on the surface structure and corrosion behavior of LDHs were studied, and the effect of the second phase on the growth of LDHs was explored. The corrosion performance was evaluated using hydrogen evolution test [37], electrochemical impedance spectroscopy (EIS), polarization curves, and immersion tests. The growth mechanism of LDHs on Mg−xCa alloys was clarified.

2 Experimental

2.1 Material preparation

The cast Mg−0.5Ca, Mg−0.8Ca and Mg−2.0Ca alloys were made by induction melting and casting under the protective gas of SF_6 (as shown in Fig. 1). Commercially pure magnesium ingots (99.9 wt.%) and Mg−30Ca master alloys were melted at 740 °C in mild steel crucible using an induction furnace. The molten metal was poured into a low carbon steel die preheated at 200 °C. The chemical composition of the as-cast Mg−xCa alloy was analyzed by energy dispersive spectrometer (EDS, JSM−7800F, FE-SEM) at three different positions and X-ray fluorescence spectrometry (XRF, ARL perform'X, China) [16].

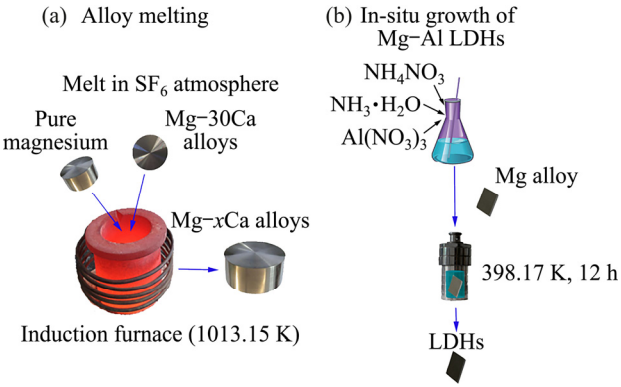

Fig. 1 Schematic diagrams illustrating alloy melting (a) and preparation of LDHs by in-situ growth method (b)

The Mg−Ca alloys were cut into specimens with size of 10 mm × 10 mm × 3 mm and 20 mm × 20 mm × 3 mm. Each specimen was ground using sandpapers to 2000#, ultrasonically washed using ethanol, and dried with cold air. For cross-sectional examinations, samples with size of 8 mm × 5 mm × 3 mm were generated with ultramicrotomy (UC; EM UC7, Leica, Germany) using a diamond knife.

2.2 Synthesis of Mg−Al LDH

Figure 1 illustrates the preparation of the

Mg−Al LDHs. The Mg−*x*Ca specimens were immersed in a solution containing 0.05 mol/L $Al(NO_3)_3$ and 0.3 mol/L NH_4NO_3, with a pH adjusted to 10.7 by adding strong ammonia water, were transferred to a Teflon-lined autoclave, and kept at 398 K for 12 h. Then, the samples were cleaned with pure water and alcohol, and dried at room temperature.

2.3 Characterization

The microstructure, chemical compositions and thickness of the films were evaluated by field emission scanning electron microscope (FE-SEM, JSM−7800 F, JEOL, Japan) equipped with energy dispersive X-ray spectrometer (EDS, INCA Energy 350, Oxford, UK). The acceleration voltage of the SEM was 10 kV. The sample was coated with gold (Au) to ensure good electrical conductivity. The crystal structure was evaluated using X-ray diffraction (XRD, D/Max 2500X, Rigaku, Japan) with a Cu target (40 kV, 150 mA) at a glancing range of 1.5°, within the range of 2θ=5°−80° and at a scanning rate of 4 (°)/min. Fourier transform infrared spectroscopy ((FT-IR; Nicolet IS5, Thermo Scientific, US) was performed in the range of 4000−400 cm^{-1}.

The corrosion resistance in 3.5 wt.% sodium chloride solution was characterized using electrochemical polarization curves and electrochemical impedance spectroscopy (EIS, CIMPS−2−Zahner, Germany). A three-electrode cell was used. The saturated calomel reference electrode (SCE), platinum foil, and the sample were respectively the reference, counter, and working electrodes. The test area was 1 cm^2. The samples were immersed in solution for 5 min prior to the electrochemical test. The amplitude of sinusoidal disturbance was 5 mV (compared with φ_{ocp}), and the polarization curve was recorded at scanning rate of 2 mV/s. EIS measurements were obtained with a frequency range from 0.001 Hz to 100 kHz. Three parallel samples in each case were tested to ensure the repeatability of the results.

The hydrogen evolution of the magnesium alloy specimens with a size of 20 mm× 20 mm was measured at room temperature in 3.5 wt.% NaCl solution [37]. Hydrogen generated by corrosion was collected every 12 h, and the volume and evolution rate were evaluated to determine the corrosion rate.

3 Results

3.1 Characteristics of Mg−*x*Ca alloys

Figure 2 presents the optical microstructures of the cast Mg−0.5Ca, Mg−0.8Ca and Mg−2.0Ca alloys, showing precipitations of intermetallic compounds around the boundaries. With increasing Ca content, the grain shape changed from dendritic to cellular, accompanied with a modest refinement to the microstructures. The grain sizes of the Mg−0.5Ca, Mg−0.8Ca and Mg−2.0Ca alloys were 70−100, 50−70 and 20−50 μm, respectively. The grain size decreased gradually from Mg−0.5Ca to Mg−2.0Ca. The Mg alloys with higher Ca content were expected to possess lower corrosion rates due to the grain refinement [38].

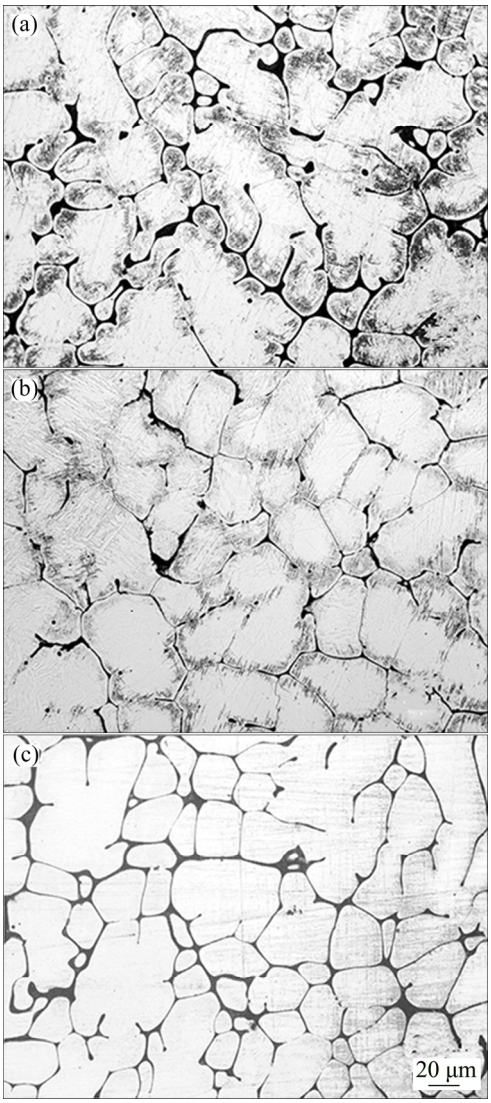

Fig. 2 Optical microstructures of Mg−*x*Ca alloys: (a) Mg−0.5Ca; (b) Mg−0.8Ca; (c) Mg−2.0Ca

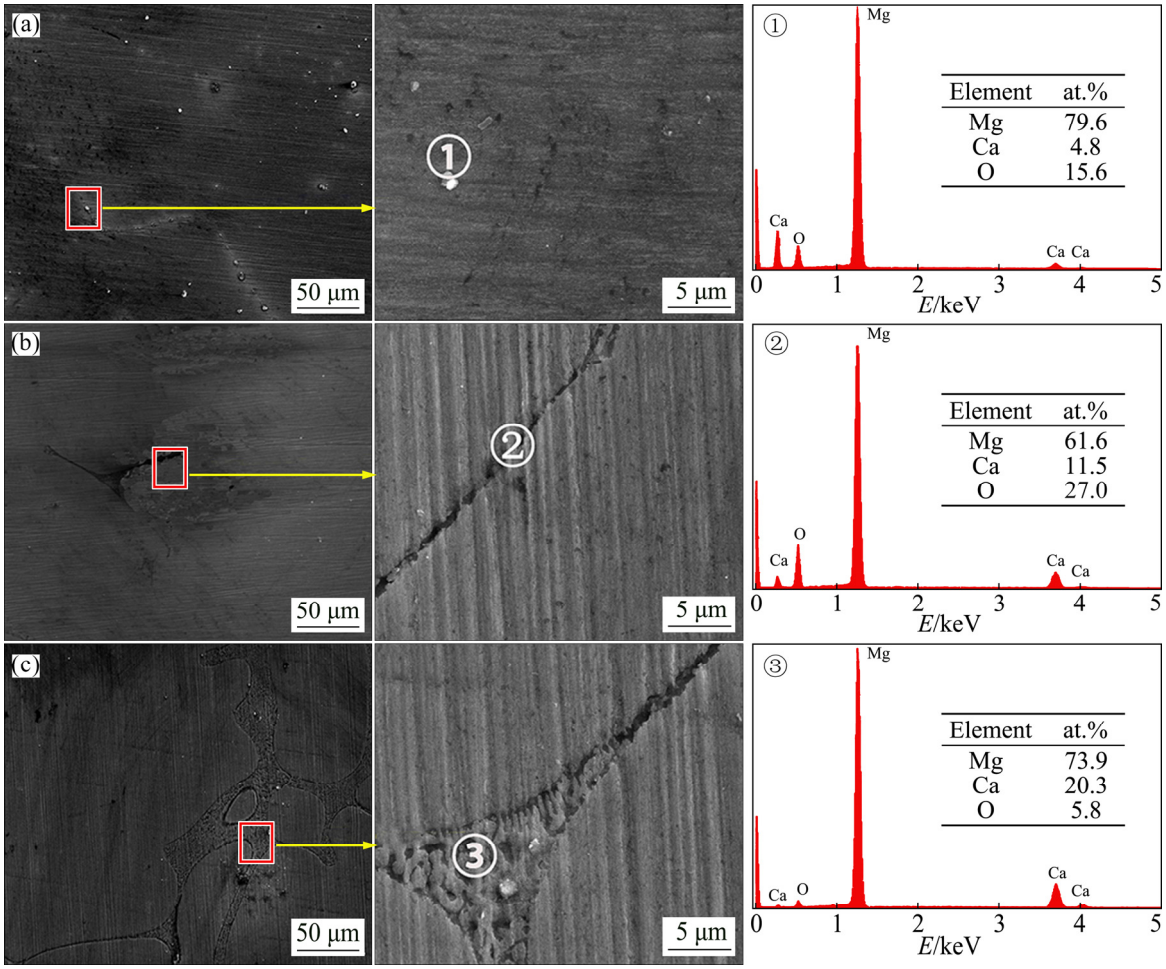

Fig. 3 SEM images at low and high magnifications and EDS spectra of Mg−*x*Ca alloys: (a) Mg−0.5Ca; (b) Mg−0.8Ca; (c) Mg−2.0Ca

Figure 3 shows the SEM images of the cast Mg−*x*Ca alloys. The *β*-Mg_2Ca particles were distributed along the grain boundaries. The wider interface (Fig. 3(c)) indicated an increased amount of *β*-Mg_2Ca particles. The XRD patterns in Fig. 4

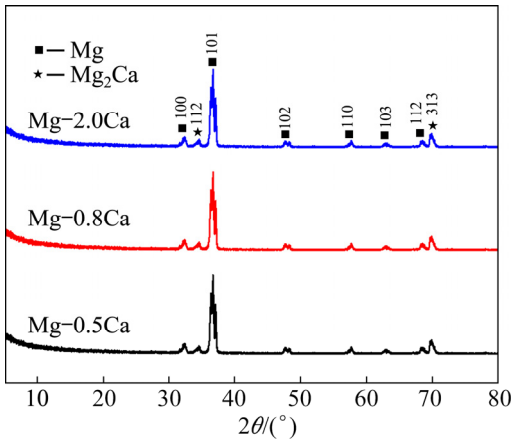

Fig. 4 XRD patterns of Mg−*x*Ca alloys

indicated that all the alloys were composed of the *β*-Mg_2Ca phase and the *α*-Mg substrate [39]. Figure 5 shows the TEM images of the as-cast Mg−0.8Ca alloy along the [0015] zone. The second phase was confirmed as Mg_2Ca. In addition, since Mg−*x*Ca alloys were smelted in a protective atmosphere, most of the oxygen in alloys came from the air oxidation. Points 1, 2 and 3 in Fig. 3 showed that the higher-calcium-content alloys had lower oxygen contents, reflecting the higher Ca content decreased the oxidation tendency. LEE et al [40] found that increasing calcium content in the Mg−*x*Ca alloys could be correlated with a weakening of the texture, indicating that calcium is an element that weakens the texture of Mg alloys. In particular, the effect of Ca on texture weakening is attributed mainly to the presence of Ca atoms in the *α*-Mg solid solution rather than the *β*-Mg_2Ca particles formed during solidification.

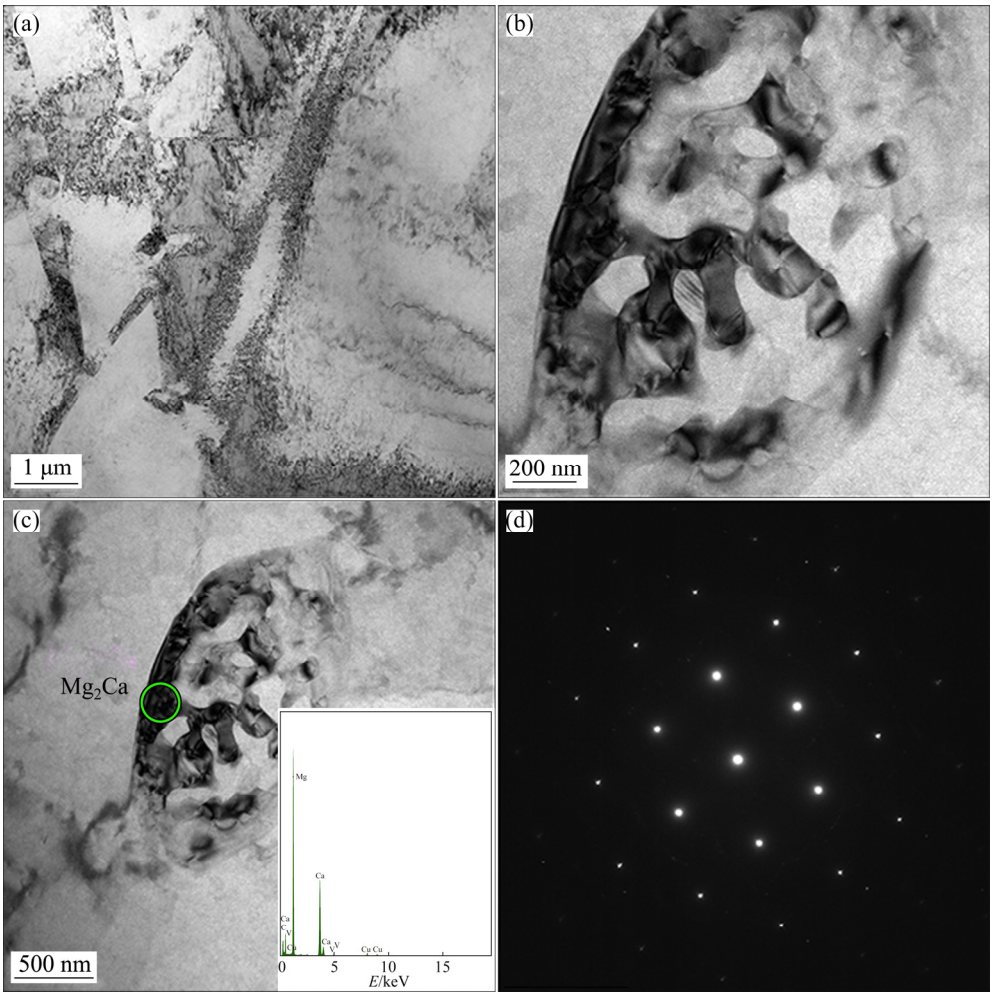

Fig. 5 TEM images of as-cast Mg−0.8Ca alloy along [0015] zone: (a) Bright field image; (b, c) Bright field images of Mg_2Ca phase and corresponding EDS spectra; (d) SAED pattern

3.2 Characteristics of MgAl−LDHs

Figure 6 shows the surface morphology of the LDHs prepared on the Mg−*x*Ca alloys with different Ca contents. The EDS spectra show the presence of the elements of oxygen (O), magnesium (Mg), aluminum (Al) and carbon (C). Because C was not contained in the reaction solution and substrate, it was concluded that the detected carbon mainly came from the dissolution of carbon dioxide in the air. The SEM images indicate that the LDHs prepared on Mg−*x*Ca alloys with different Ca contents had some abnormal bulges with different sizes, which were unevenly distributed on the surface. These petal-shaped bumps with typical LDHs structure were larger in size, sparsely arranged and their vertical orientation to the substrate was reduced compared with conventional LDHs. The amount of these bulges increased with increasing Ca content, showing that the growth rate of the LDHs was faster at these points than on the surrounding substrate. Since Mg ions in this study came from the dissolution of the substrate, the growth rate of LDHs located in these locations would be accelerated only by the fast dissolution. More specifically, a large number of corrosion micro-galvanic cells were most probably formed by the potential difference (PD) between the second phase and the alloy substrate. The potential of the second phase was negative as the cathode, and that of the magnesium alloy substrate was positive as the anode [41], causing the substrate to dissolve faster than the Mg_2Ca. Simultaneously, compared to relative normal regions, the surrounding substrate of the second phase with more numerous crystal defects caused by the presence of Mg_2Ca resulted in the heterogeneity of electrochemical composition and higher energy, and thus led to the fastest dissolution rate of the three (the second phase, the magnesium substrate and the surrounding substrate of the second phase). Finally, the regions with the

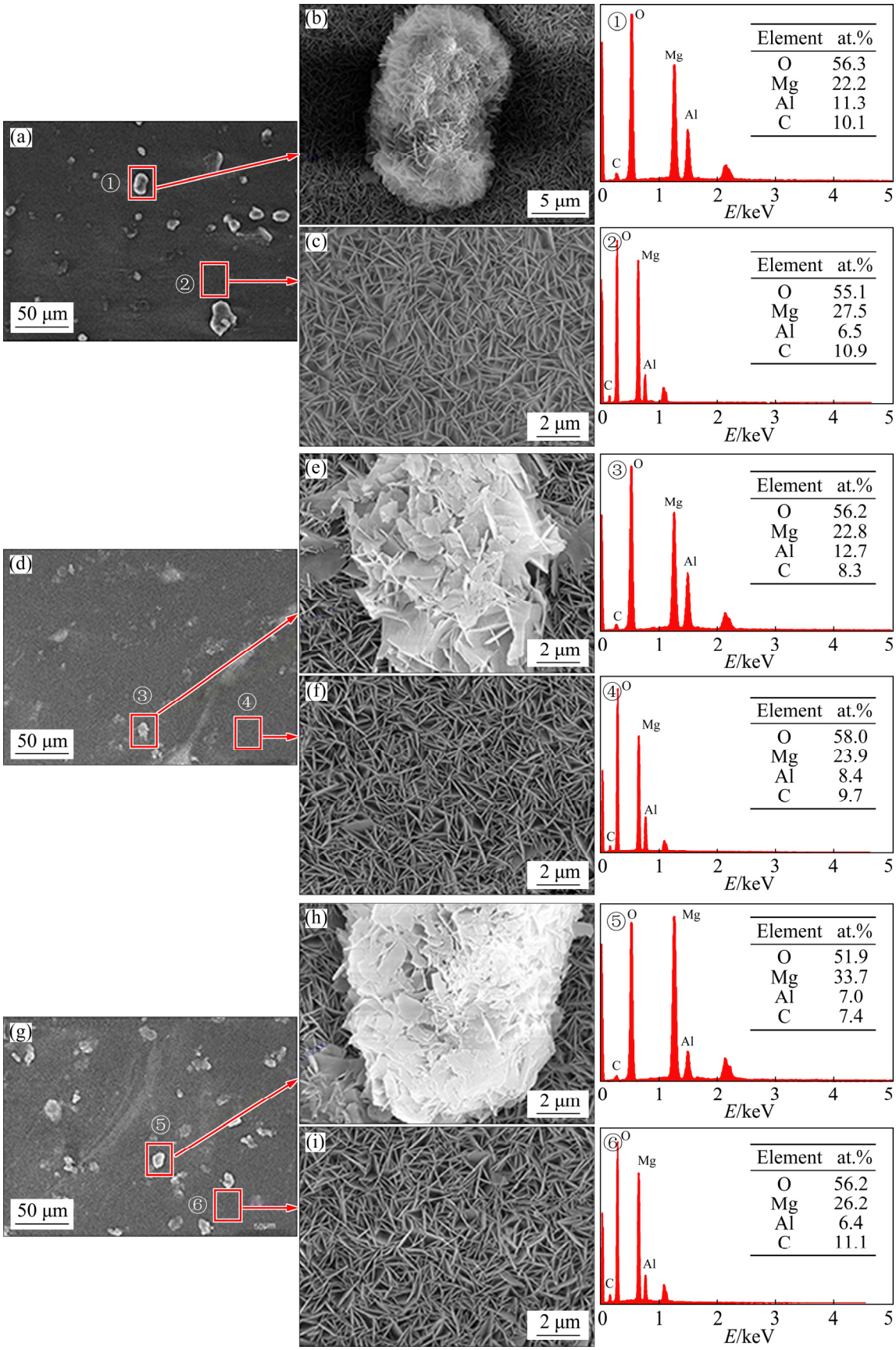

Fig. 6 SEM images and EDS spectra of LDHs prepared on Mg−*x*Ca alloy surface: (a−c) LDHs/Mg−0.5Ca; (d−f) LDHs/Mg−0.8Ca; (g−i) LDHs/Mg−2.0Ca

fastest dissolution rate interacted with the second phase with the slowest dissolution rate to produce the bulge. Therefore, these bulges may be at Mg_2Ca-rich particles in these rather impure alloys, which was consistent with the results in Fig. 6. Moreover, the above also indicates that the second phase promoted the growth of LDHs by making the substrate dissolve faster.

In the normal regions, the LDHs of the three samples were continuous and complete without obvious cracks and holes, and the density of nanosheets was almost the same. Figures 6(c, f, i) indicate that the regular nanosheets were compactly arranged without obvious pores, presenting the typical lamellar structure of LDHs and growing perpendicularly to the substrate surface. The EDS spectra indicate that the LDHs in normal region were composed of O, Mg and Al, and their molar ratio was about 8.5:4:1. The protrusions were also composed of these three elements. Compared with normal region, their compositions were almost the same. Therefore, the Ca content did not change the chemical composition of the LDHs.

Figure 7 shows SEM images of the sectional morphology of LDHs prepared on Mg−0.5Ca, Mg−0.8Ca and Mg−2.0Ca alloys, indicating that the film thickness was relatively uniform for all specimens. However, there were some anomalous areas with large fluctuations, indicating that the growth rate of LDHs in such locations was faster. The EDS spectra indicate that the concentration of Ca was larger than that of Mg, and these locations corresponded to the second phase of the magnesium alloy. Since LDHs prepared by an in-situ growth depended on the dissolution of substrate [3], due to the micro-galvanic corrosion [41], the dissolution rate of substrate next to the second phase was faster, so the thickness of the second phase region was larger. Therefore, the second phase (Mg_2Ca) was favorable for the growth of LDH film, consistent with previous observations. Increasing Ca content increased the number of the second phase particles, and the interface between the film and the substrate was much more uniform.

The thickness of LDH films on the Mg−0.5Ca alloy surface was about 1.5 μm (Fig. 7(a)), and the interface between the LDH films and the substrate was smooth, which indicated that the second phase was tiny and dispersedly distributed. When the content of Ca was 0.8%, the thickness of LDH films was about 1.7 μm (Fig. 7(b)). The unevenness of the interface between the film and the substrate

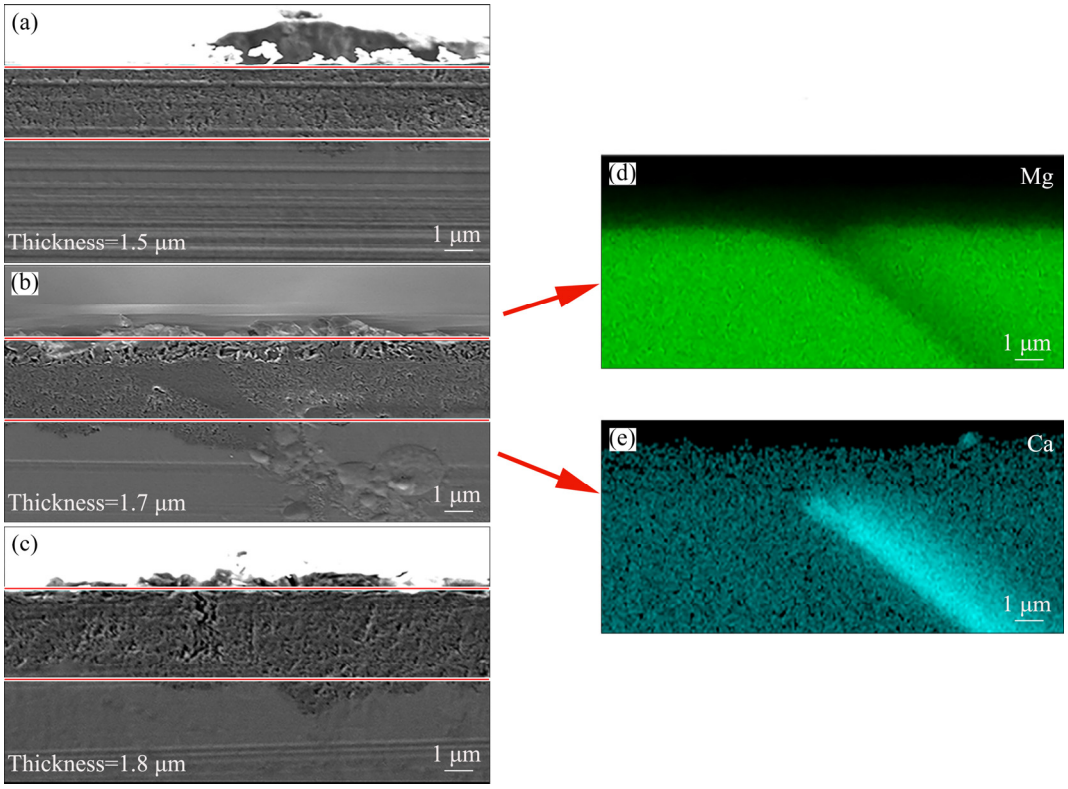

Fig. 7 Cross-sectional morphologies of LDHs prepared on Mg−*x*Ca alloy surface: (a) LDHs/Mg−0.5Ca; (b) LDHs/Mg−0.8Ca; (c) LDHs/Mg−2.0Ca

increased slightly, and the thickness was increased as well. Figures 7(b, d, e) showed that the content of the second phase increased and the substrate dissolved quickly, promoting the growth of LDHs, which was consistent with previous observations. When the Ca content was 2.0%, the thickness of the films increased further to 1.8 μm (Fig. 7(c)), indicating that the increase of the second phase increased the fluffy growth of LDHs. Namely, the second phase promoted the growth of LDHs but did not favor its densification.

Figure 8 shows the XRD patterns of the LDHs prepared on the Mg−Ca alloys with different Ca contents. The characteristic reflections of (003) and (006) (at 2θ around 11.7° and 23.3°, respectively) show that the LDHs had been synthesized on the Mg−xCa alloys. The presence of magnesium hydroxide ($Mg(OH)_2$) indicated the presence of magnesium hydroxide in the films. In addition, the typical diffraction peaks of (003) and (006) indicate that the LDHs had a complete layered structure and good crystal structure [42].

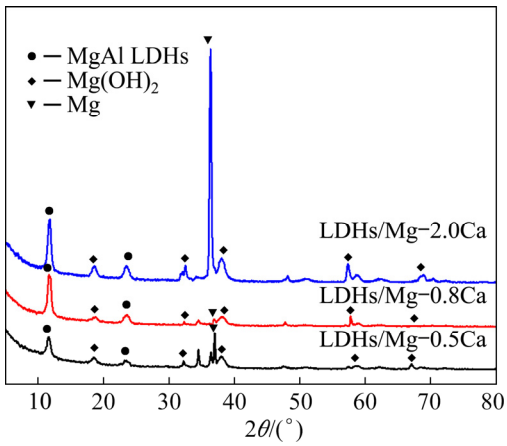

Fig. 8 XRD patterns of LDHs on Mg−xCa Alloys

The most intensive peak was from Mg. With increasing Ca content, the intensity of the characteristic peaks of MgAl LDHs and $Mg(OH)_2$ increased, indicating that increasing Ca content promoted the formation of the LDHs, which was also consistent with the results in Fig. 7. The Ca content in the Mg alloy had an important influence on the formation of LDHs. In addition, increasing Ca content did not cause any significant shift in the position of the characteristic peaks of MgAl LDHs, indicating that the spacing between crystal planes was approximately the same.

Figure 9 shows FT-IR spectra corresponding to the coating on the Mg−Ca alloys with different Ca contents. The absorption peaks at 3693, 3460 and 1640 cm^{-1} corresponded to H—O—H stretching vibration, O—H symmetric vibration, and bending vibration of water molecules in the LDHs, respectively. These weak peaks were due to the stretching vibration of hydroxyl groups in water molecules, meaning that there were some water molecules in the LDHs or on the surface. The absorption peaks around 1380 cm^{-1} originated from the presence of interlayer nitrate. The asymmetric stretching peaks of NO_3^- in three kinds of samples were obvious and wide. When the Ca content was 0.5%, the asymmetric stretching peak of NO_3^- near 1380 cm^{-1} was the narrowest of the three. When Ca content was 2.0%, the asymmetric stretching peak of NO_3^- became sharp and strong, which corresponded to the increase of the thickness of LDH films. The characteristic peaks at 450−751 cm^{-1} originated from the absorption peaks caused by lattice vibration of Al—O, Mg—O—Al and Mg—O bonds. When the Ca content was 2.0%, the obvious Al—OH peak indicated the crystallization of LDHs.

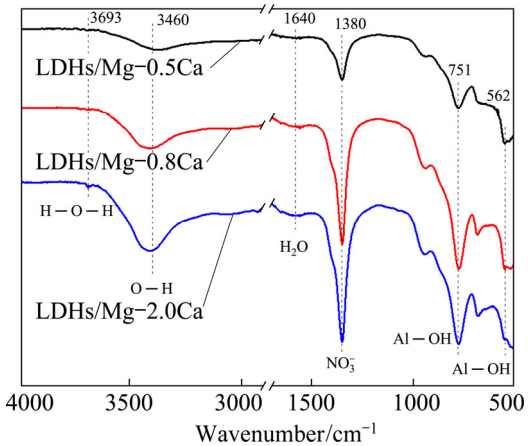

Fig. 9 FT-IR spectra of LDHs on Mg−xCa alloys

3.3 Corrosion performance

3.3.1 Electrochemical tests

Figure 10 shows typically potentiodynamic polarization curves of the LDHs prepared on Mg−0.5Ca, Mg−0.8Ca and Mg−2.0Ca alloys in 3.5 wt.% NaCl aqueous solution. The corrosion parameters of the LDHs prepared on Mg−xCa alloys are summarized in Table 1. The corrosion potentials of LDHs prepared on Mg−0.5Ca, Mg−0.8Ca and Mg−2.0Ca alloys were −18, −167 and −347 mV (vs SCE), respectively, and the

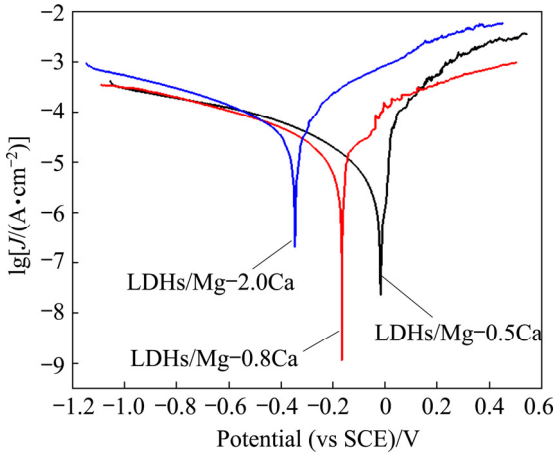

Fig. 10 Polarization potentiodynamic curves recorded in 3.5 wt.% NaCl solution of various samples

Table 1 Corrosion parameters of LDHs prepared on Mg−*x*Ca alloy

Sample	φ_{corr}(vs SCE)/ mV	J_{corr}/ (μA·cm^{-2})	P_i/ (mm·a^{-1})
LDHs/Mg−0.5Ca	−18.16	86.21	1.97
LDHs/Mg−0.8Ca	−167.30	12.46	0.28
LDHs/Mg−2.0Ca	−346.82	58.28	1.33

corrosion current densities were 86.21, 12.46 and 58.28 μA/cm^2, respectively. The corrosion rate was evaluated using

$$P_i=\frac{3.27\times10^{-3}AJ_{corr}}{n\rho} \quad (1)$$

where A is the relative atomic mass of magnesium (A=24.305), n is the valence of Mg cation (n=2) and ρ represents the density of magnesium (ρ= 1.738 g/cm^3).

The corrosion rates for LDHs prepared on Mg−0.5Ca, Mg−0.8Ca and Mg−2.0Ca alloys covered with LDHs were 1.97, 0.28 and 1.33 mm/a, respectively, indicating that the Ca content influenced the corrosion rate of the Mg−*x*Ca alloys coated with the LDHs. Increasing Ca content increased the amount of second phase particles, causing the formation of thicker more-corrosion-resistant LDHs and fluffy LDHs (as shown in Fig. 7), and increasing the micro-galvanic corrosion. Due to these factors, the Mg−0.8Ca/LDHs showed the lowest corrosion rate.

Figure 11 shows EIS spectra obtained for the different samples in 3.5 wt.% NaCl solution. The frequency−impedance Bode diagram (Fig. 11(b)) indicates that the impedance increased with decreasing frequency. The impedance values at high frequency terminal capacitive reactance arc were similar, and all exceeded 1000 cm^2, showing that LDHs had good dielectric properties and high charge flow resistance, which can protect the substrate. Moreover, the curve of LDHs/Mg−2.0Ca was lower than that of other samples, although the difference was not large. The LDHs/Mg−0.8Ca had the lowest corrosion rate.

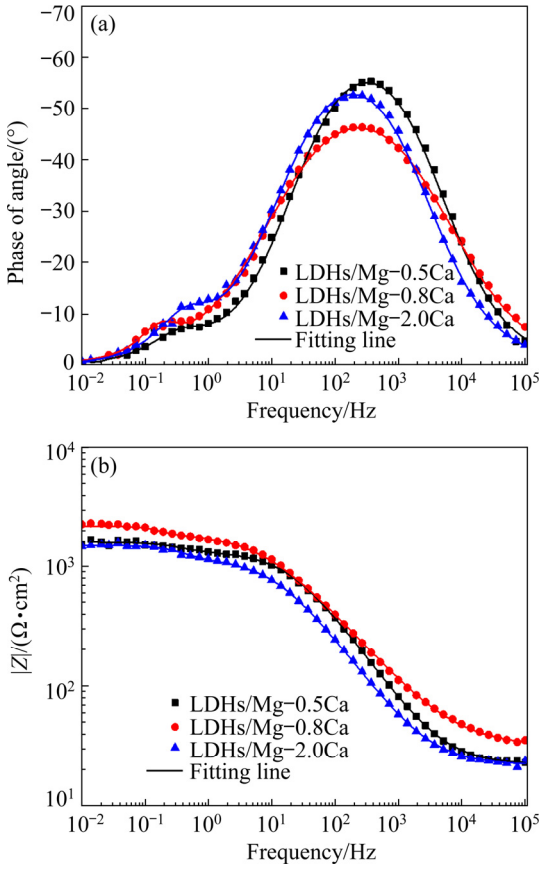

Fig. 11 EIS spectra obtained for different samples in 3.5 wt.% NaCl solution: (a) Bode phase of angle; (b) Bode impedance

Typical Bode plots after immersion for 7 d in 3.5 wt.% NaCl solution are presented in Fig. 12. The impedance values at 1×10^{-2} Hz decreased, indicating that the corrosion rate increased. The impedance values of LDHs/Mg−0.5Ca and LDHs/Mg−0.8Ca decreased greatly at low frequency, indicating that their corrosion rate greatly increased. Compared with other samples, LDHs/Mg−2.0Ca was more corrosion resistant.

The equivalent circuit of LDHs on the sample is given in Fig. 13. R_s represents electrolyte resistance, CPE_{LDH} and R_{LDH} represent capacitance

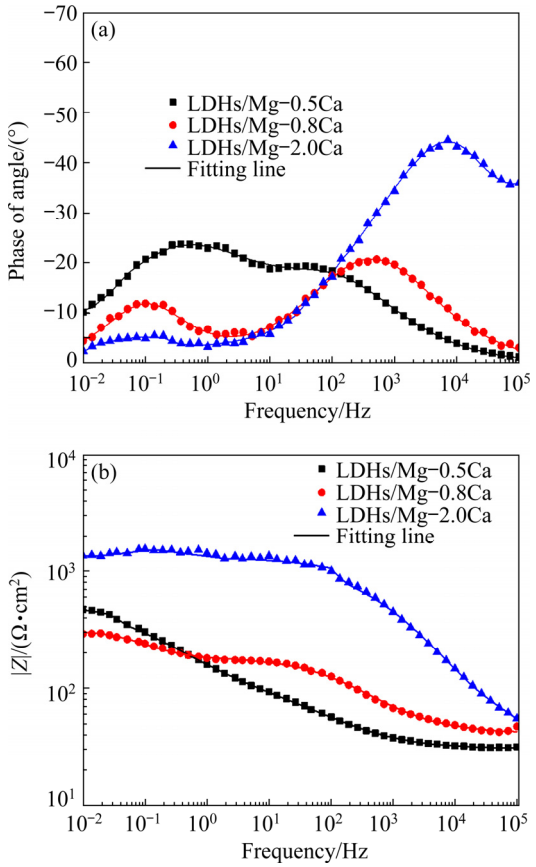

Fig. 12 Impedance spectra of LDHs prepared on Mg−*x*Ca alloys surface after 7 d immersion in 3.5 wt.% NaCl solution: (a) Bode phase of angle; (b) Bode impedance

and resistance of external films layer, respectively. CPE_{Mg-xCa} and R_{Mg-xCa} refer to capacitance and charge transfer resistance between the substrate and the films, respectively. Tables 2 and 3 indicate that

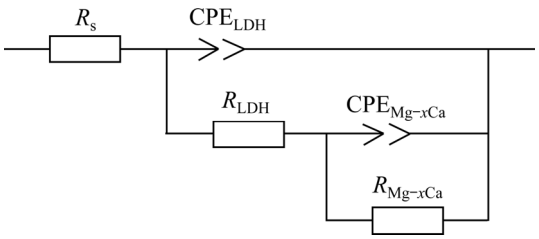

Fig. 13 Equivalent circuits used to fit spectra in Figs. 11 and 12

the LDHs grown on Mg−*x*Ca alloy had high R_{Mg-xCa} and R_{LDH} values. The higher R_{Mg-xCa} and R_{LDH} values can be attributed to the sealing effect of LDHs and the compact internal structure. Therefore, the corrosion rate of the Mg−*x*Ca alloy was effectively decreased by the in-situ growth of LDHs.

Figure 14 shows the polarization curves of the LDHs/Mg−Ca alloys immersed in 3.5 wt.% NaCl solution for 7 d. Table 4 shows their corrosion potential φ_{corr} and corrosion current density J_{corr}. The polarization potential of the samples after immersion decreased, and the corrosion current density of LDHs/Mg−0.5Ca and LDHs/Mg−0.8Ca alloys increased, while the corrosion current density of LDHs/Mg−2.0Ca decreased slightly. This is because the produced thicker corrosion products adhered to the surface to provide some protection, but their corrosion resistance was poor. The corrosion potentials of LDHs/Mg−0.5Ca, LDHs/Mg−0.8Ca and LDHs/Mg−2.0Ca were −425.77, −110.05 and −464.71 mV (vs SCE), the corrosion current densities were 141.54, 294.56 and

Table 2 Fitted parameters for EIS spectrum depicted in Fig. 11

Sample	R_s/ ($\Omega\cdot cm^2$)	CPE_{LDH}		R_{LDH}/ ($\Omega\cdot cm^2$)	CPE_{Mg-xCa}		R_{Mg-xCa}/ ($\Omega\cdot cm^2$)	χ^2
		Q_t/($S\cdot s^n\cdot cm^{-2}$)	n		Q_t/($S\cdot s^n\cdot cm^{-2}$)	n		
LDHs/Mg−0.5Ca	22.07	1.88×10^{-5}	0.76	1.34×10^{3}	2.00×10^{-3}	1	2.41×10^{2}	6.50×10^{-3}
LDHs/Mg−0.8Ca	31.26	3.83×10^{-5}	0.64	1.95×10^{3}	3.96×10^{-3}	1.26	2.38×10^{2}	3.61×10^{-3}
LDHs/Mg−2.0Ca	22.27	3.33×10^{-5}	0.74	1.16×10^{3}	1.19×10^{-3}	1	3.33×10^{3}	9.87×10^{-3}

Table 3 Fitted parameters for EIS spectrum depicted in Fig. 12

Sample	R_s/ ($\Omega\cdot cm^2$)	CPE_{LDH}		R_{LDH}/ ($\Omega\cdot cm^2$)	CPE_{Mg-xCa}		R_{Mg-xCa}/ ($\Omega\cdot cm^2$)	χ^2
		Q_t/($S\cdot s^n\cdot cm^{-2}$)	n		Q_t/($S\cdot s^n\cdot cm^{-2}$)	n		
LDHs/Mg−0.5Ca	30.5	4.77×10^{-4}	0.60	56.33	3.57×10^{-3}	0.44	7.37×10^{2}	6.04×10^{-3}
LDHs/Mg−0.8Ca	41.06	1.24×10^{-4}	0.61	1.42×10^{2}	1.41×10^{-2}	0.81	1.33×10^{2}	6.58×10^{-3}
LDHs/Mg−2.0Ca	22.27	1.85×10^{-5}	0.50	1.94×10^{2}	9.98×10^{-8}	0.94	1.13×10^{3}	5.42×10^{-3}

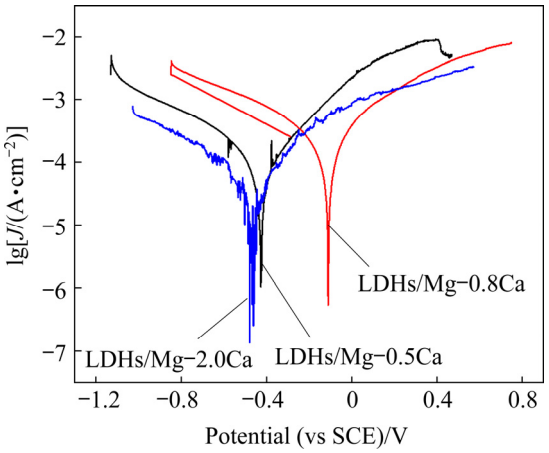

Fig. 14 Tafel polarization curves of LDHs/Mg−*x*Ca alloy after 7 d immersion in 3.5 wt.% NaCl solution

Table 4 Corrosion potential and current density of LDHs/Mg−*x*Ca alloy after 7 d immersion in 3.5 wt.% NaCl solution

Sample	φ_{corr} (vs SCE)/V	J_{corr}/(μA·cm^{-2})	P_i/(mm·a^{-1})
LDHs/Mg−0.5Ca	−425.77	141.54	3.24
LDHs/Mg−0.8Ca	−110.05	294.56	6.73
LDHs/Mg−2.0Ca	−464.71	41.28	0.94

41.28 μA/cm^2, and the corrosion rates were 3.24, 6.73 and 0.94 mm/a, respectively. The corrosion current densities of LDHs/Mg−0.5Ca and LDHs/Mg−0.8Ca increased by one order of magnitude, indicating that the corrosion rates of LDHs/Mg−0.8Ca increased significantly after immersion for 7 d. The reason is that the LDHs had been destroyed, and the active corrosion inhibition ability had declined or even disappeared, so that they could not prevent the penetration of corrosive media to contact with the substrate. The corrosion current of LDHs/Mg−2.0Ca decreased, probably because the corrosion products blocked the pores of fluffy LDHs, combined with the thickest LDHs in three kinds of alloys, thus leading to the reduction of corrosion rate. In addition, a higher Ca content in Mg−2.0Ca alloy refined the grain, so the Mg−2.0Ca alloy showed better corrosion resistance.

3.3.2 Hydrogen evolution results

The hydrogen evolution results show that the hydrogen gas volume increased with increasing immersion time. Figure 15(a) shows that no hydrogen was released in a short time, indicating that the films provided the protection for substrate.

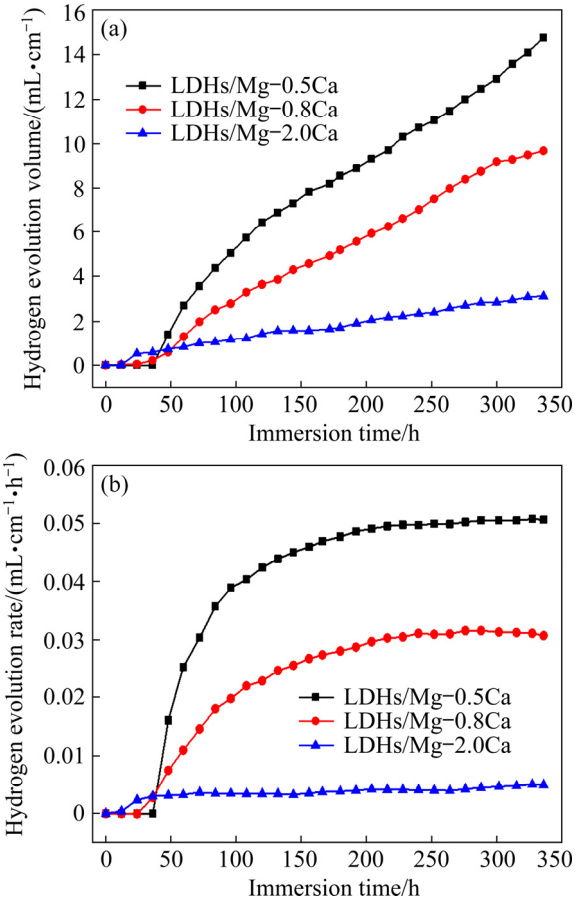

Fig. 15 Hydrogen evolution volume (a) and hydrogen evolution rate (b) of LDHs/Mg−*x*Ca in 3.5wt.% NaCl with soaking time

After that, the film lost some corrosion protection, and the hydrogen release rate increased. The hydrogen evolution of LDHs/Mg−2.0Ca was the lowest, while that of Mg−0.5Ca was the largest. In comparison, the LDHs on Mg−2.0Ca alloy presented a more durable corrosion protection as a result of grain refinement associated with the increase of Ca content. The rate of hydrogen evolution in Fig. 15(b) indicates that for 100 h of immersion, initially the rate of hydrogen evolution for all samples increased rapidly, and reached a steady state rate of 3.24 (Mg−0.5Ca), 6.73 (Mg−0.8Ca) and 0.94 mm/a (Mg−2.0Ca). With increasing immersion time, some corrosion products generated later adhered to the alloy substrate, providing some protection. However, the volume of hydrogen release and the rate of hydrogen evolution of LDHs/Mg−2.0Ca were somewhat less than those of the other two alloys, which may indicate that LDHs/Mg−2.0Ca had better corrosion resistance, which was consistent

with the Tafel results, or may indicate that the purity of this alloy was better than that of the other alloys.

3.3.3 Corrosion morphologies

Figure 16 shows the SEM images and EDS spectra of LDH films on Mg−*x*Ca alloys after immersion in 3.5 wt.% NaCl solution for 7 d. Figure 16(a) shows that there was no hexagonal nanosheets on the surface, but a large number of white and flocculent corrosion products, with the main elements of O, Mg and C. A small amount of Cl was detected, indicating that the LDHs film had lost its barrier to corrosive ions. The basic morphology of LDHs was clear in Fig. 16(b), but after immersion, the hexagonal lamellar structure of LDHs deformed, the density decreased greatly, and the vertical orientation with the substrate was also decreased. Figure 16(c) shows that the corrosion products were spherical, with many pores of different sizes. Generally speaking, the corrosion of Mg−0.2Ca alloy was slight, showing good durability and corrosion resistance.

4 Discussion

Mg−*x*Ca alloys consisted of *α*-Mg phase and *β*-Mg_2Ca phase (Fig. 4). Due to the difference of the potential of *α*-Mg and *β*-Mg_2Ca phases, *β*-Mg_2Ca phase was a cathode and accelerated the dissolution of *α*-Mg phase, generating a wide range of micro-currents on the surface of Mg−*x*Ca alloys. The dissolution rate of the *α*-Mg phase was faster than that of the *β*-Mg_2Ca phase, so that the pH value for the LDHs deposition was more easily reached. However, the diffusion rate of the solution in the *α*-Mg phase was slow, especially far away from the *β*-Mg_2Ca phase, resulting in relatively difficult coating in these places. The LDHs were formed in the surrounding area of the second phase first, then on *α*-Mg phase, and finally on the *β*-Mg_2Ca phase, which was consistent with the previous theoretical analysis results (Fig. 3). When there were more *β*-Mg_2Ca phases, the size of LDHs conversion film changed greatly (Fig. 6).

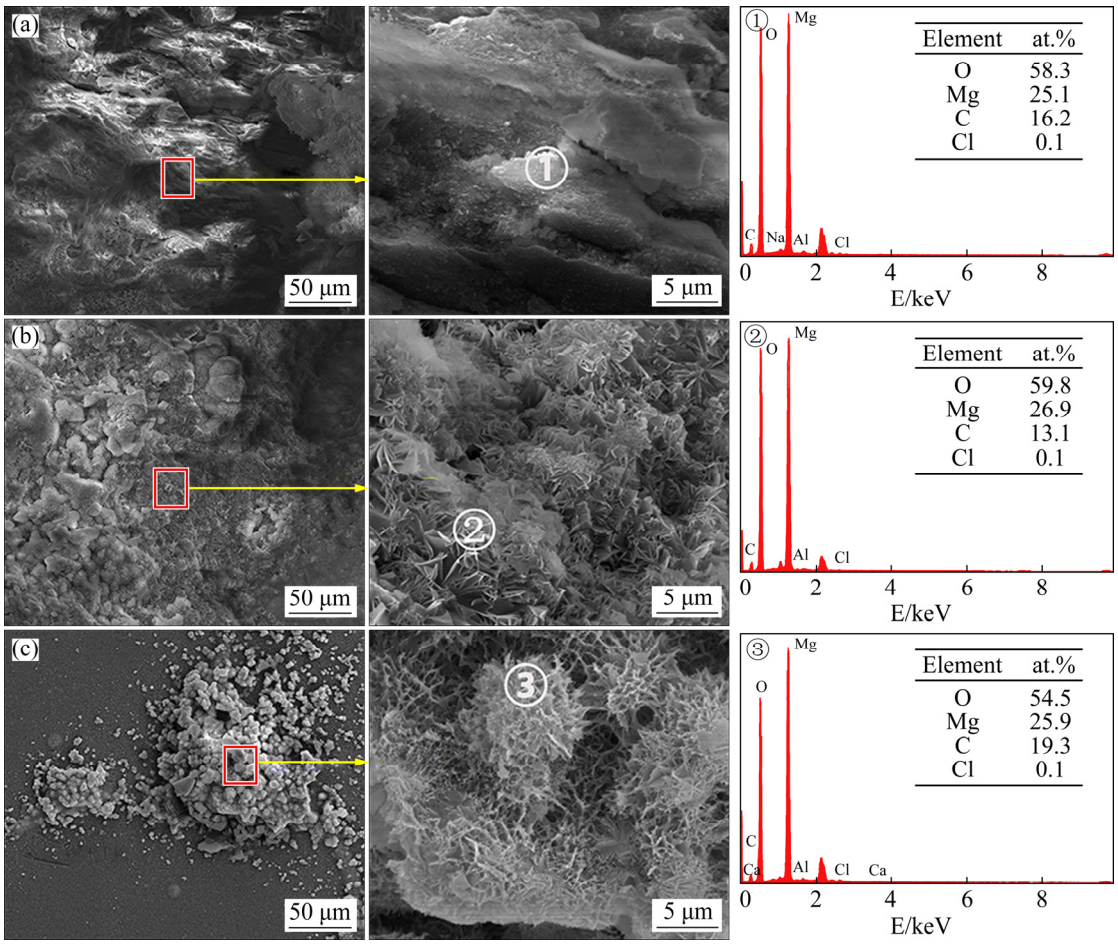

Fig. 16 Morphologies and EDS spectra of LDHs prepared on surface of Mg−*x*Ca alloy after 7 d immersion in 3.5 wt.% NaCl solution: (a) LDHs/Mg−0.5Ca; (b) LDHs/Mg−0.8Ca; (c) LDHs/Mg−2.0Ca

With increasing calcium content, the amount of the second phase increased, and the grains were refined. In the process of grain refinement, due to the increase of the amount of the second phase and the existence of stress, many crystal defects like dislocations, twins and textures were produced, resulting in the inhomogeneity of electrochemical composition and high energy. Due to different microstructures, the electrochemical activity of the alloys showed an obvious difference. For regions with high electrochemical activity, the film was easier to form, because these regions are those with the fastest alloy dissolution [43]. At the same time, these high electrochemical active regions can easily reach the pH value needed for LDHs growth, meaning that the grain boundaries, dislocations, twins and textures make the growth of LDHs easier. Namely, the second phase can promote the growth of LDHs.

Under self-corrosion, on the account of the potential difference between the phase of the magnesium alloy and the impurity, the second phase and the rich magnesium phase were the cathode and anode of micro-galvanic corrosion, respectively. Because of the potential of Mg−*x*Ca alloys, the *β*-Mg_2Ca phase as cathode accelerated the dissolution of the *α*-Mg phase in alkaline solution, forming LDHs on the surface of the Mg−Ca alloys.

Since the magnesium ions in the LDHs prepared in this study come from the dissolution of the substrate, the formation mechanism of LDHs film on the Mg−*x*Ca alloys with different Ca contents was as follows: (1) The substrate provided metal cation of Mg^{2+} for the formation of LDHs, and the reaction solution provided metal cation of Al^{3+}. The surface undulation due to the second phase (Mg_2Ca) increased the contact area between substrate and solution, facilitating the reaction. (2) The surface of the magnesium alloy was corroded, releasing Mg^{2+} which reacted with OH^- to form $Mg(OH)_2$, deposited on the surface. This entire process is shown as the following reactions [44]:

$$Mg+H^++H_2O\rightarrow Mg^{2+}+OH^-+H_2\uparrow \quad (2)$$

$$Mg^{2+}+2OH^-\rightarrow Mg(OH)_2\downarrow \quad (3)$$

In this process, some magnesium ions were replaced by aluminum ions to form $Mg_2Al(OH)_7$ and other compounds, so that the surface of the magnesium substrate became more uneven and undulating. MORIDI et al [45] showed that an uneven surface facilitated film formation. Therefore, the surface undulations caused by the second phase and reactive corrosion were beneficial to the growth of LDHs. (3) Compounds containing more Al such as $Mg_2Al(OH)_7$ could combine with Al^{3+} in solution to form $Mg_6Al_2(OH)_{18}\cdot 4.5H_2O$. (4) NO_3^{3-} was inserted between layers as an anion to form MgAl−LDH structure.

LDHs can sense the appearance of corrosive ions in the surrounding environment [41,46], such as chloride ions, and then the interlayer anions are released to absorb corrosive ions (Fig. 17). Therefore, LDHs can decrease the corrosion rate. Since the second phase and the substrate formed corrosive microcells and accelerated the dissolution of the substrate, the LDHs at the second phase were thicker and more nitrate ions were inserted into the interlayer so that the anti-corrosion property was improved by effectively absorbing the corrosive ions. After the film was destroyed, the corrosion resistance of LDHs/Mg−2.0Ca was obviously better than that of the other two systems.

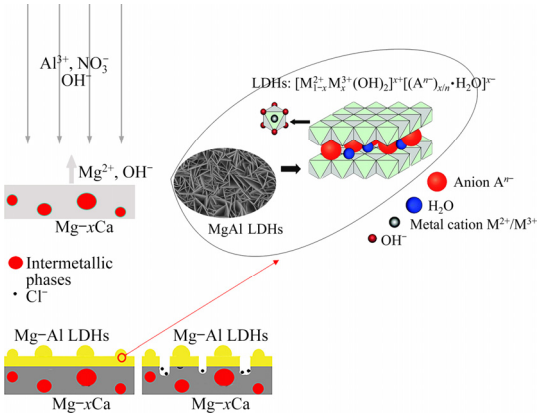

Fig. 17 Schematic diagram illustrating corrosion mechanism of MgAl LDHs

5 Conclusions

(1) LDHs, growing directly on the Mg−*x*Ca alloys by the in-situ growth method, were vertically grown and compactly arranged without obvious pores.

(2) The LDHs prepared by the in-situ growth depended on the dissolution of the Mg−*x*Ca alloy substrate, especially the surrounding area of Mg_2Ca phase. Increasing the amount of second phase particles increased the dissolution rate, resulting in forming thicker and fluffy LDHs. However, the

LDHs nanocrystals were sparsely arranged and petal-shaped, and their vertical orientation on the substrate was lost.

(3) The thickness of the LDHs was affected by the content of Ca element in the Mg−*x*Ca alloys. Increasing Ca content increased the film thickness.

(4) The Mg−*x*Ca alloys coated with LDHs exhibited different corrosion rates. LDHs/Mg−0.8Ca showed the lowest corrosion rate on account of the dual effects of Mg_2Ca, but after 7 d of immersion, the LDHs/Mg−2.0Ca showed the lowest corrosion rate.

Acknowledgments

This work was supported by the National Natural Science Foundation of China (No. 51971040), the Fundamental Research Funds for the Central Universities, China (No. 2020CDJQY-A007), China Postdoctoral Science Foundation (Nos. 2017M620410, 2018T110942), and the Chongqing Postdoctoral Scientific Research Foundation, China (No. Xm2017010).

References

[1] ATRENS A, JOHNSTON S, SHI Zhi-ming, DARGUSCH M S. Viewpoint-understanding Mg corrosion in the body for biodegradable medical implants [J]. Scripta Materialia, 2018, 154: 92−100.

[2] GNEDENKOV A S, SINEBRYUKHOV S L, MASHTALYAR D V, GNEDENKOV S V. Protective properties of inhibitor-containing composite coatings on a Mg alloy [J]. Corrosion Science, 2016, 102: 348−354.

[3] ZHANG Gen, WU Liang, TANG Ai-tao, MA Yan-long, SONG Guang-ling, ZHENG Da-jiang, JIANG Bin, ATRENS A, PAN Fu-sheng. Active corrosion protection by a smart coating based on a MgAl-layered double hydroxide on a cerium-modified plasma electrolytic oxidation coating on Mg alloy AZ31 [J]. Corrosion Science, 2018, 139: 370−382.

[4] MAKKAR P, SARKAR S K, PADALHIN A R, MOON B G, LEE Y S, LEE B T. In vitro and in vivo assessment of biomedical Mg−Ca alloys for bone implant applications [J]. Journal of Applied Biomaterials & Functional Materials, 2018, 16: 126−136.

[5] CHAI Y F, HE C, JIANG B, FU J, JIANG Z T, YANG Q S, SHENG H R, HUANG G S, ZHANG D F, PAN F S. Influence of minor Ce additions on the microstructure and mechanical properties of Mg−1.0Sn−06Ca alloy [J]. Journal of Materials Science Technology, 2020, 37: 26−37.

[6] SONG G L, ATRENS A. Understanding magnesium corrosion—A framework for improved alloy performance [J]. Advanced Engineering Materials, 2003, 5: 837−858.

[7] ATRENS A, SONG G L, LIU M, SHI Z, CAO F, DARGUSCH M S. Review of recent developments in the field of magnesium corrosion [J]. Advanced Engineering Materials, 2015, 17: 400−453.

[8] ATRENS A D, GENTLE I, ATRENS A. Possible dissolution pathways participating in the Mg corrosion reaction [J]. Corrosion Science, 2015, 92: 173−181.

[9] ATRENS A, SONG G L, CAO F, SHI Z, BOWEN P K. Advances in Mg corrosion and research suggestions [J]. Journal of Magnesium and Alloys, 2013, 1: 177−200.

[10] SONG G, ATRENS A. Corrosion mechanisms of magnesium alloys [J]. Advanced Engineering Materials, 1999, 1: 11−33.

[11] ZHANG Shao-xiang, ZHANG Xiao-nong, ZHAO Chang-li, LI Jia-nan, SONG Yang, XIE Chao-ying, TAO Hai-rong, ZHANG Yan, HE Yao-hua, JIANG Yao, BIAN Yu-jun. Research on an Mg−Zn alloy as a biodegradable biomaterial [J]. Acta Biomaterialia, 2010, 6: 626−640.

[12] XU L P, YU G N, ZHANG E, PAN F, YANG K. In vivo corrosion behavior of Mg−Mn−Zn alloy for bone implant application [J]. Journal of Biomedical Materials Research A, 2007, 83: 703−711.

[13] LI Zi-jian, GU Xu-nan, LOU Si-quan, ZHENG Yu-feng. The development of binary Mg−Ca alloys for use as biodegradable materials within bone [J]. Biomaterials, 2007, 29: 1329−1344.

[14] LEE C D, KANG C S, SHIN K S. Effect of galvanic corrosion between precipitate and matrix on corrosion behavior of as-cast magnesium−aluminum alloys [J]. Metals and Materials, 2000, 6: 351−358.

[15] SALAHSHOOR M, GUO Y B. Surface integrity of biodegradable magnesium−calcium orthopedic implant by burnishing [J]. Journal of the Mechanical Behavior of Biomedical Materials, 2011, 4: 1888−1904.

[16] HARANDI S E, MIRSHAHI M, KOLEINI S, IDRIS M H, JAFARI H, KADIR M R A. Effect of calcium content on the microstructure, hardness and in-vitro corrosion behavior of biodegradable Mg−Ca binary alloy [J]. Materials Research, 2013, 16: 11−18.

[17] GU C D, YAN W, ZHANG J L, TU J P. Corrosion resistance of AZ31B magnesium alloy with a conversion coating produced from a choline chloride−urea based deep eutectic solvent [J]. Corrosion Science, 2016, 106: 108−116.

[18] ZENG R C, QI W C, SONG Y W, HE Q K , GUI H Z, HAN E H. In vitro degradation of MAO/PLA coating on Mg−1.21Li−1.12Ca−1.0Y alloy [J]. Frontiers of Materials Science, 2014, 8: 343−353.

[19] ECHEVERRY-RENDON M, DUQUA V, QUINTERO D C, HARMSEN M, ECHEVERRIA F. Novel coatings obtained by plasma electrolytic oxidation to improve the corrosion resistance of magnesium-based biodegradable implants [J]. Surface and Coatings Technology, 2018, 354: 28−37.

[20] GUO Lian, WU Wei, ZHOU Yong-feng, ZHANG Fen, ZENG Rong-chang, ZENG Jian-min. Layered double hydroxide coatings on magnesium alloys: A review [J]. Journal of Materials Science and Technology, 2018, 34: 1455−1466.

[21] ZHANG Gen, WU Liang, TANG Ai-tao, WENG Bo, ATRENS A, MA S, LIU Lei, PAN Fu-sheng. Sealing of anodized magnesium alloy AZ31 with MgAl layered double hydroxides layers [J]. RSC Advances, 2018, 8: 22−48.

[22] BESTETTI M, CAVALLOTTI P L, DA FORNO A, POZZI S.

Anodic oxidation and powder coating for corrosion protection of AM60B magnesium alloys [J]. Transactions of the Institute Metal Finishing, 2007, 85: 316−319.

[23] GUI L Y, ZENG R C, LI S Q, ZHANG F, HAN E H. Corrosion resistance of layer-by-layer assembled polyvinylpyrrolidone/polyacrylic acid and amorphous silica films on AZ31 magnesium alloys [J]. RSC Advances, 2016, 6: 63107−63116.

[24] LIU L J, LI P P, ZOU Y H, LUO K J, ZHANG F, ZENG R C, LI S Q. In vitro corrosion and antibacterial performance of polysiloxane and poly(acrylic acid)/gentamicin sulfate composite coatings on AZ31 alloy [J]. Surface and Coatings Technology, 2016, 291: 7−14.

[25] ZENG R C, LIU L J, LI S Q, ZOU Y H, ZHANG F, YANG Y, GUI H Z, HAN E H. Self-assembled silane film and silver nanoparticles coating on magnesium alloys for corrosion resistance and antibacterial applications [J]. Acta Metallurgica Sinica (English Letters), 2013, 26: 681−686.

[26] SAHOO P, GADHARI P. Electroless nickel−phosphorus composite coatings: A review [J]. International Journal of Manufacturing, Materials and Mechanical Engineering, 2016, 6: 14−50.

[27] MOSA J, NAVARRO R, APARICIO M. Active corrosion inhibition of mild steel by environmentally-friendly Ce-doped organic–inorganic sol–gel coatings [J]. RSC Advances, 2016, 6: 39577−39586.

[28] PENG F, WANG D H, CAO H L, LIU X Y. Loading 5-fluorouracil into calcined Mg/Al layered double hydroxide on AZ31 via memory effect [J]. Materials Letters, 2017, 213: 383−386.

[29] ALIBAKHSHI E, GHASEMI E, MAHDAVIAN M, RAMEZANZADEH B, FARASHI S. Active corrosion protection of Mg−Al−PO_4^{3-} LDH nanoparticle in silane primer coated with epoxy on mild steel [J]. Journal of the Taiwan Institute of Chemical Engineers, 2017, 75: 248−262.

[30] LI Y D, LI S M, ZHANG Y, YU M, LIU J H. Enhanced protective Zn−Al layered double hydroxide film fabricated on anodized 2198 aluminum alloy [J]. Journal of Alloys and Compounds, 2015, 630: 29−36.

[31] KUZNETSOV B, SERDECHNOVA M, TEDIM J, STARYKEVICH M, KALLIP S, OLIVEIRA M P, HACK T, NIXON S, FERREIRA M G S, ZHELUDKVICH M L. Sealing of tartaric sulfuric (TSA) anodized AA2024 with nanostructured LDH layers [J]. RSC Advances, 2016, 6: 13942−13952.

[32] SERDECHNOVA M, MOHEDANO M, KUZNETSOV B, MENDIS C L, STARYKEVICH M, KARPUSHENKOV S, TEDIM J, FERREIRA M G S, BLAWERT C, ZHELUDKEVICH M L. PEO coatings with active protection based on in-situ formed LDH-nanocontainers [J]. Journal of the Electrochemical Society, 2016, 164: 36−45.

[33] DOU B J, WANG Y Q, ZHANG T, LIU B, SHAO Y W, MENG G Z, WANG F H. Growth behaviors of layered double hydroxide on microarc oxidation film and anti-corrosion performances of the composite film [J]. Journal of the Electrochemical Society, 2016, 163: 917−927.

[34] MOHEDANO M, SERDECHNOVA M, STARYKEVICH M, KARPUSHENKOV S, BOUALI A C, FERREIRA M G S, ZHELUDKEVICH M L. Active protective PEO coatings on AA2024: Role of voltage on in-situ LDH growth [J]. Materials and Design, 2017, 120: 36−46.

[35] CHEN Jing, WU Liang, DING Xing-xing, LIU Qiang, DAI Xu, SONG Jiang-feng, JIANG Bin, ATRENS A, PAN Fu-sheng. Effects of deformation processes on morphology, microstructure and corrosion resistance of LDHs films on magnesium alloy AZ31 [J]. Journal of Materials Science & Technology, 2019, 10: 1005−0302.

[36] ZHANG Xiao-chen, ZHONG Feng, LI Xuan-peng, LIU Bin, ZHANG Chun-yan, BUHE Bateer, ZHANG Tao, MENG Guo-zhe, WANG Fu-hui. The effect of hot extrusion on the microstructure and anti-corrosion performance of LDHs conversion coating on AZ91D magnesium alloy [J]. Journal of Alloys and Compounds, 2019, 788: 756−767.

[37] SONG G L, ATRENS A, STJOHN D. An hydrogen evolution method for the estimation of the corrosion rate of magnesium alloys [J]. Magnesium Technology, 2011. DOI:10.1002/9781118805497.ch44.

[38] HARANDI S E, MIRSHAHI M, KOLEINI K, IDRIS M H, JAFARI H, KADIR M R A. Effect of calcium content on the microstructure, hardness and in-vitro corrosion behavior of biodegradable Mg−Ca binary alloy [J]. Materials Research, 2013, 16: 11−18.

[39] LI Zi-jian, GU Xu-nan, LOU Si-quan, ZHENG Yu-feng. The development of binary Mg−Ca alloys for use as biodegradable materials within bone [J]. Science Direct Biomaterials, 2008, 29: 1329−1344.

[40] LEE Jong-Youn, YUN Young-Su, KIM Won-Tae, KIM Do-Hyang. Twinning and texture evolution in binary Mg−Ca and Mg−Zn alloys [J]. Metals and Materials International, 2014, 20: 885−891.

[41] WU Liang, DING Xing-xing, ZHENG Zhi-cheng, TANG Ai-tao, ZHANG Gen, ATRENS A, PAN Fu-sheng. Doublely-doped Mg−Al−Ce−$V_2O_7^{4-}$ LDH composite film on magnesium alloy AZ31 for anticorrosion [J]. Journal of Materials Science & Technology, 2021, 64: 62−72.

[42] WU Liang, YANG Dan-ni, ZHANG Gen, ZHANG Zhi, ZHANG Sheng, TANG Ai-tao, PAN Fu-sheng. Fabrication and characterization of Mg−M layered double hydroxide films on anodized magnesium alloy AZ31 [J]. Applied Surface Science, 2018, 431: 177−186.

[43] PAWAR S, SLATER T J A, BURNETT T L, ZHOU X, SCAMANS G M, FAN Z, THOMPSON G E, WITHERS P J. Crystallographic effects on the corrosion of twin roll cast AZ31 Mg alloy sheet [J]. Acta Materialia, 2017, 133: 90−99.

[44] LIU B S, KUANG Y F, CHAI Y S, FANG D Q, ZHANG M G, WEI Y H. Degradation research of protective coating on AZ91D Mg alloy components via simulated contamination [J]. Journal of Magnesium and Alloys, 2016, 4: 220−229.

[45] MORIDI A, RUAN Hai-hui, ZHANG Liang-chi, LIU Mei. On the dependence of surface undulation on film thickness [J]. Journal of Physics and Chemistry of Solids, 2014, 75: 500−504.

[46] CHEN Jing, WU Liang, DING Xing-xing, LIU Qiang, DAI Xu, SONG Jiang-feng, JIANG Bing, ATRENS A, PAN Fu-sheng. Effects of deformation processes on morphology, microstructure and corrosion resistance of LDHs films on magnesium alloy AZ31 [J]. Journal of Materials Science & Technology, 2021, 64: 10−20.

Mg−Ca 合金表面的原位层状双氢氧化物：Ca 在镁合金中的作用

夏 雨[1]，吴 量[1,2]，姚文辉[1,2]，郝 蒙[1]，陈 晶[1]，张 诚[3]，吴 涛[1]，
谢治辉[4]，宋江凤[1,2]，蒋 斌[1,2]，麻彦龙[5]，潘复生[1,2]

1. 重庆大学 材料科学与工程学院 机械传动国家重点实验室，重庆 400044；
2. 重庆大学 国家镁合金材料工程技术研究中心，重庆 400044；
3. 长江师范学院 材料科学与工程学院 重庆市无机特种功能材料重点实验室，重庆 408100；
4. 西华师范大学 化学化工学院 化学合成与污染控制四川省重点实验室，南充 637002；
5. 重庆理工大学 材料科学与工程学院，重庆 400054

摘 要：采用原位生长法在铸态 Mg−*x*Ca (*x*=0.5，0.8，2.0，质量分数，%)合金上制备 Mg−Al 双层氢氧化物(LDHs)。与镁基体相比，该合金具有良好的耐蚀性能。研究第二相(Mg_2Ca)对 LDHs 的影响机理。随着 Ca 含量的增加，Mg_2Ca 的数量增加，导致 Mg−*x*Ca 合金的晶粒尺寸减小，腐蚀速率降低。第二相数量的增加和晶粒细化促进 LDHs 的生长，从而降低 Mg−*x*Ca 合金的腐蚀速率。同时，较高的 Mg_2Ca 数量使 LDHs 变得蓬松。由于第二相(Mg_2Ca)对 LDHs 的双重影响，LDHs/Mg−0.8Ca 的腐蚀速率最低。

关键词：Mg−Ca 合金；Mg−Al 双层氢氧化物；耐蚀性能；原位生长；自愈合

(Edited by Bing YANG)